Pressure-induced large valence transitions in Yb–Cu binary intermetallic systems

Hitoshi Yamaoka,[1,*] Ayako Ohmura,[2,†] Naohito Tsujii,[3] Hirofumi Ishii,[4]
Nozomu Hiraoka,[4] Hitoshi Sato,[5] and Masahiro Sawada[5]

[1] *RIKEN SPring-8 Center, 1-1-1 Kouto, Mikazuki, Sayo, Hyogo 679-5148, Japan*
[2] *Faculty of Science, Niigata University, Niigata 950-2181, Japan*
[3] *Research Center for Materials Nanoarchitectonics (MANA), National Institute for Materials Science, 1-2-1 Sengen, Tsukuba, Ibaraki 305-0047, Japan*
[4] *National Synchrotron Radiation Research Center, Hsinchu 30076, Taiwan*
[5] *Hiroshima Synchrotron Radiation Center, Hiroshima University, Higashi-Hiroshima, Hiroshima 739-0046, Japan*

(Dated: March 18, 2024)

Electronic and crystal structures of YbCu, $YbCu_2$, and $YbCu_{6.5}$ under pressure were studied by high-resolution x-ray absorption spectroscopy and x-ray diffraction. We found pressure-induced large valence transitions on the order of 0.3 in these Yb compounds. YbCu exhibited a first-order transition with a sudden change in the Yb-valence at 4 GPa, at which a structural transition was not accompanied. With further increasing pressure, YbCu shows a structural transition from the FeB-type to the cubic CsCl-type structure around 10 GPa, where the Yb valence increases only gradually. In $YbCu_2$, a structural transition was not observed up to 11.8 GPa, while the Yb valence shows a rapid increase around 4–7 GPa, indicating a significant change in the electronic structure. Anomalous re-entrant valence transition to lower valence state was found at low pressures of 3–4 GPa in $YbCu_{6.5}$ without the structural phase transition. It is suggested that the anomaly in $YbCu_{6.5}$ possibly correlated to the electronic structure of the Cu d band. On the other hand, we found that these anomalous large changes in the Yb valences were linked to anomalies in crystal structures although there were no structural phase transitions. Complementary to the measurements of the PFY-XAS spectra under pressure, we performed x-ray absorption spectroscopy at the Cu-L_3 absorption edge and measured the valence band spectra at ambient pressure.

I. INTRODUCTION

In rare-earth compounds, some of the elements such as Yb, Eu, Sm, and Ce often show the valence instability between the two charge states [1–3]. The $4f$ electrons of these elements have a localized nature, while the electronic state of the $4f$ electrons in the compounds is the result of the hybridization of the $4f$ electrons with conduction (c) electrons (c–f hybridization) which is characterized by the Kondo temperature (T_K) [4]. The valence of the rare-earth elements of these compounds is a measure of the c–f hybridization and the Kondo temperature, which could be controlled by chemical substitution, temperature, and pressure.

In Yb compounds, Yb^{3+} state is favored under pressure because of the smaller ion radius of Yb^{3+} ions compared to that of Yb^{2+} ions. Pressure increases the Yb valence with decreasing the c–f hybridization and induces the magnetically-ordered state through a quantum critical point (QCP) with increasing the Yb valence [5]. This behavior has been described within the Doniac's phase diagram and the Anderson model [6, 7]. Interestingly, in Yb compounds a theory predicts that further increase of the pressure decreases the Yb valence and there may be a second QCP because of the increase of the hybridization [8]. This pressure range was on the order of more than around 100 GPa and the electronic structures of Yb compounds have not been explored so far in this high-pressure range.

Recently, on the other hand, direct measurements of the Yb valence under pressures have revealed that some Yb compounds showed an anomalous decrease of the Yb valence with pressure at low pressures. In $YbCu_{4.5}$ a first-order valence transition to the divalent Yb state was found around 0.6–2.7 GPa [9]. This valence transition was accompanied by the structural transition at the same pressure range. Furthermore, in the cubic $YbCu_5$-based compounds the Yb valence was found to decrease with pressure without structural phase transition at low pressures less than 10 GPa, indicating a pressure-induced crossover from a localized $4f^{13}$ state to the valence fluctuation regime, which was not expected for Yb systems with the conventional c–f hybridization [10]. A similar pressure-induced anomaly of the Yb valence has been also observed in $YbInCu_4$-based compounds [11]. Anomalies of the decrease of the Yb valence under pressure in these systems have been found to correspond to anomalies in the crystal structure.

In this paper, we performed a systematic study of the electronic and crystal structures of the Yb–Cu binary intermetallic systems, the compositions of YbCu, $YbCu_2$, $YbCu_{4.5}$, $YbCu_5$, and $YbCu_{6.5}$ [12–17, 19–21]. The purpose of the paper is to clarify the pressure dependences in the crystal and electronic structures of these compounds which have not been explored yet. One of the physically interesting matters is whether the pressure-induced anomaly in the Yb-valence is a general phenomenon or not. Thus, it is vital to explore Yb systems that show the

* Corresponding author: yamaoka@spring8.or.jp
† Corresponding author: ohmura@phys.sc.niigata-u.ac.jp

pressure-induced valence decrease at low pressure, other than $YbCu_{4.5}$, cubic $YbCu_5$-based, and $YbInCu_4$-based compounds [9–11]. To measure the electronic structures of YbCu, $YbCu_2$, and $YbCu_{6.5}$ under pressure, we employ high-resolution x-ray absorption spectroscopy with a partial fluorescence mode (PFY-XAS) at the Yb-L_3 absorption edge [22–24]. Pressure dependences of the crystal structures were also measured. We found large changes in the valence of the order of 0.3 under pressure in YbCu and $YbCu_2$.

Lawrence *et al.* systematically measure the temperature dependence of Yb valence while changing X for $YbXCu_4$ (X = Ag, Cd, In, Mg, Tl, Zn), and discussed how the slow crossover of Yb valence changed. In $YbXCu_4$, the crystal structure did not change even if X is changed, but in $YbCu_x$, the crystal structure changed when the Cu composition was changed as described below, and thus we also systematically measured the pressure dependence of the crystal structures. In this study, we found a common feature between anomalous changes in the Yb valences and anomalies in crystal structures.

Complementary to the measurements of the electronic structure of the Yb site under pressure, we performed x-ray absorption spectroscopy at the Cu-L_3 absorption edge to measure that of the Cu site at ambient pressure. Additionally, the valence band spectra were measured at ambient pressure [25].

II. EXPERIMENTS

Polycrystalline samples of YbCu and $YbCu_2$ were prepared by melting the pure elements of Yb (99.9%) and Cu (99.99%) in a closed Nb tube. The Nb tubes were sealed by an arc furnace under argon atmosphere. Then, the tubes were sealed in evacuated quartz tubes and were heated in an electric furnace. For YbCu, the quartz tube was heated at 1223 K for 6 hours and cooled to 873 K, at which the sample was annealed for 48 hours. For $YbCu_2$, the quartz tube was heated at 1273 K for 1 hour, and was homogenized at 1003 K for 12 hours.

Polycrystalline samples of $YbCu_{4.5}$ and $YbCu_{6.5}$ were prepared by melting the elements in an arc furnace under argon atmosphere, and subsequently annealing. Slightly excess amounts of Yb were added to compensate the loss of Yb during the arc melting. The melted ingots were wrapped with tantalum foils and were sealed in evacuated quartz tubes. Then the samples were annealed by heating the tubes at 1023 K for 2 weeks.

Homogeneities and chemical compositions of $YbCu_x$ samples were confirmed by the scanning electron microprobe (SEM) and the electron probe micro analysis (EPMA). The backscattered electron images (BEI-COMPO) of the samples indicate that the samples were homogeneous and phase pure. The chemical compositions were almost in agreement with the stoichiometry of $YbCu_x$. The chemical composition observed for YbCu, $YbCu_2$, and $YbCu_{4.5}$ (Yb_2Cu_9), $YbCu_5$, and $YbCu_{6.5}$ were $Yb_{47.4}Cu_{52.6}$, $Yb_{31.1}Cu_{68.9}$, $Yb_{18.2}Cu_{81.8}$, $YbCu_{5.13}$, and $Yb_{14.8}Cu_{85.2}$, respectively. In particular, the chemical composition for $YbCu_{4.5}$ was Yb 18.2% and Cu 81.8%, which is very close to those of $YbCu_{4.5}$. Therefore, the neighboring phases, such as $YbCu_{4.4}$ and $YbCu_{4.25}$, are not relevant in the present experiment [33, 34]. Crystal structure and physical parameters of YbCu, $YbCu_2$, $YbCu_{3.5}$, $YbCu_{4.5}$, and $YbCu_{6.5}$ are summarized in table I [9, 12, 15–17, 19–21, 26–32]. The effective magnetic moments of $YbCu_x$ with higher Cu content at $x \geqq 3.5$ suggest nearly the Yb^{3+} valence state because the effective moment of a free Yb^{3+} ion is $4.54\mu_B$.

Measurements of the PFY-XAS spectra were performed at room temperature at the Taiwan beamline BL12XU, SPring-8 [35]. A Johann-type spectrometer equipped with a spherically bent Si(620) crystal (radius of ∼1 m) was used to analyze the Yb emission of $3d_{5/2} \rightarrow 2p_{3/2}$ de-excitation following a $2p_{3/2} \rightarrow 5d$ excitation with a solid state detector. The intensities of all sample spectra are normalized by the intensity of the incident beam monitor of an ion chamber just before the sample. The overall energy resolution was estimated to be about 1 eV around the emitted photon energy of 7400 eV from the elastic scattering. The high-pressure conditions were realized using a diamond anvil cell (DAC) with a Be-gasket and the pressure-transmitting medium was silicone oil. The pressure was measured by the ruby fluorescence method [36, 37]. A Be-gasket with 3 mm in diameter and approximately 100 μm thick pre-indented to approximately 40–50 μm thick. The diameter of the sample chamber in the gasket was approximately 120 μm and the diamond anvil culet size was 300 μm. We used the Be gasket in-plane geometry where both incoming and outgoing x-ray beams passed through the Be gasket.

Pressure dependence of the x-ray diffraction patterns was measured at BL12B2, SPring-8, using a CCD detection system at room temperature. For pressure generation, a 3-pin plate diamond anvil cell (Plate DAC, Almax easyLab) was used with silicon oil as the pressure-transmitting medium. We take an arrangement of both incoming and outgoing x-ray beams passing through the diamonds with an incident photon energy of $h\nu = 18$ keV ($\lambda = 0.6888$ Å). A two-dimensional image of the CCD system was integrated by using the FIT2D program [38]. The quality of the XRD patterns at high-pressure phase of YbCu was not good for the Rietveld analyses and thus we fitted them by the La Bail method also using the Jana2006 program. For $YbCu_2$ and $YbCu_{6.5}$, lattice constants and atomic positions were refined by the Rietveld method using the Jana 2006 program [39–41]. Since the quality of the XRD patterns for YbCu was not good for the Rietveld method, we obtained its lattice constants analyzed by the Le Bail method also using the Jana2006 program. Examples of the fits are shown in the Supplemental Materials [25]. Vacuum ultra-violet PES was performed at the beam line BL-7, the Hiroshima

TABLE I. Crystal structure and physical parameters of YbCu, $YbCu_2$, $YbCu_{3.5}$, $YbCu_{4.5}$, and $YbCu_{6.5}$. μ_{eff}, γ, and T_K are the effective magnetic moment, the specific heat coefficient, and the Kondo (or characteristic) temperature, respectively. The values of the Yb valence with an asterisk mark (*) were the values at ambient pressure estimated from the PFY-XAS spectra in this study. $YbCu_{6.5}$ is related to the $CaCu_5$ structure including 18% Ca site occupied by pairs of Cu atoms [13]. $YbCu_{4.5}$ is based on $AuBe_5$-type substructures with approximately 4570 and 2780 atoms per unit cell [33]. The crystal structure of $YbCu_{4.5}$ was solved using x-ray diffraction and high-resolution transmission electron microscopy by Cerny *et al.* [20]: a mono-clinically distorted 7×7×6.5 superstructure of the cubic $AuBe_5$ structure type with 7448 atoms per unit cell.

	YbCu	$YbCu_2$	$YbCu_{3.5}$	$YbCu_{4.5}$	$YbCu_5$	$YbCu_{6.5}$
Crystal structure	Orthorhombic	Orthorhombic	unknown		cubic	Hexagonal
Type	$FeB^{a,b,c}$	$CeCu_2{}^b$		$AuBe_5{}^{c,d}$	$AuBe_5{}^c$	$CaCu_5{}^{c,e}$
Yb valence	2.89^a, 2.37^f	2.39^f, 2.5^g	2.89^f, 2.7^b	2.96^f, 2.85^b, 2.95^h	2.97^i	2.40^f
Yb valence (present study)	2.05*	2.20*				2.41*
μ_{eff} (μ_B)			4.12^j, 4.3^k	4.22^j, 4.36^f, 3.9^k	4.55^l	
γ (mJ/mol K^2)		6.8^m	90^b, 310^k	600^n, 635^o	$550^{l,p}$	
				740^q (0.82 GPa)		
T_K (K)				15^f	60^l	

a: Ref. [17], b: Ref. [18], c: Ref. [19], d: Ref. [20], e: Ref. [13] f: Ref. [15], g: Ref. [26], h: Ref. [9], i: Ref. [27], j: Ref. [12], k: Ref. [28], l: Ref. [16], m: Ref. [29], n: Ref. [30] o: Ref. [21], p: Ref. [31], q: Ref. [32],

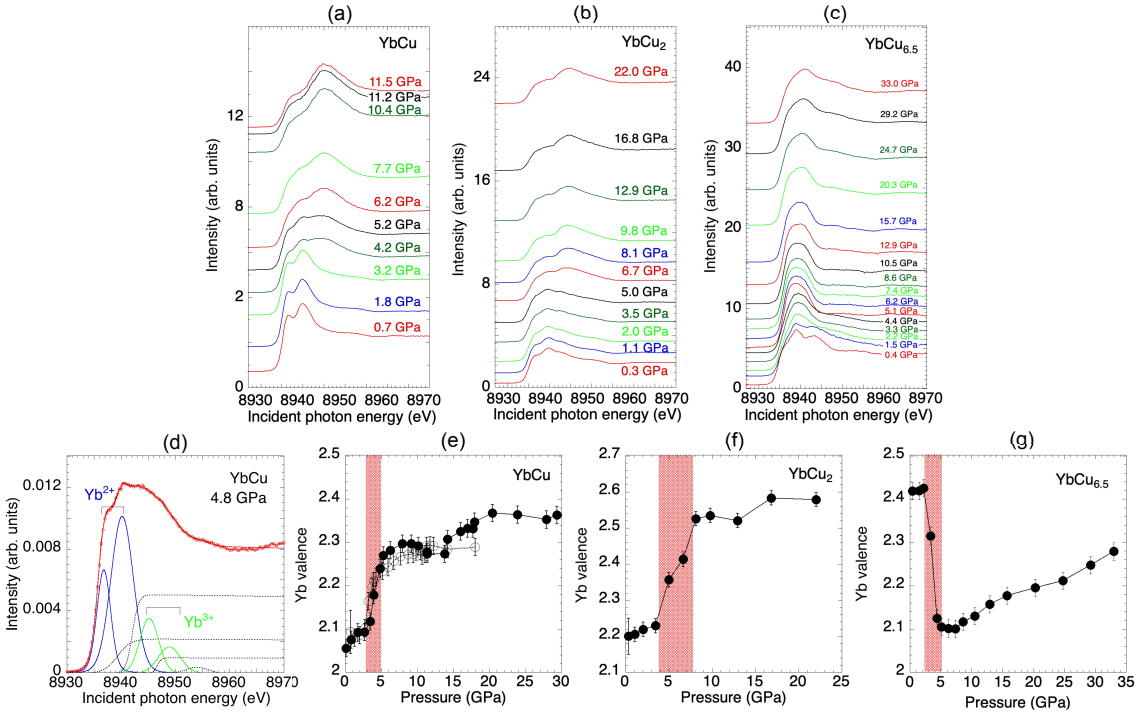

FIG. 1. (Color online) (a), (b), and (c) Pressure dependence of the PFY-XAS spectra for (a) YbCu, (b) $YbCu_2$, and (c) $YbCu_{6.5}$, respectively. (d) A fit example of the PFY-XAS spectra of YbCu at 4.8 GPa. (e), (f), and (g) Pressure dependence of the Yb valence of YbCu, $YbCu_2$, and $YbCu_{6.5}$, respectively. In (e) two independent measurements for YbCu are shown as closed and open circles. In (e), (f), and (g) shaded areas correspond to the pressure range where the valence transitions occur.

Synchrotron Radiation Center (HiSOR), equipped with a hemispherical electron-energy analyzer (Gammadata-Scienta SES-2002). The energy resolution (ΔE) was set to approximately 150 meV at $h\nu = 182$ eV under the vacuum pressure below 10^{-8} Pa. The Fermi edge of Au evaporated on the sample holder was used to calibrate the binding energy. Samples were fractured in vacuum just before the measurements. The energy resolution and the Fermi level are determined with a fit of the Fermi edge of Au using a convolution of Gaussian and Fermi-Dirac functions.

X-ray absorption spectra at the Cu-L absorption edge

were measured at BL-14 at HiSOR with the total electron yield mode, where the samples were fractured under the vacuum [42]. The energy resolution was set to be approximately less than 0.2 eV around 930 eV.

III. RESULTS AND DISCUSSION

A. XAS at the Yb-L_3 absorption edge

Pressure dependence of the PFY-XAS spectra of YbCu, $YbCu_2$, and $YbCu_{6.5}$ are shown in Figs. 1 (a), 1 (b), and 1 (c), respectively. In Fig. 1 (d) we show an example of the fit of YbCu at 4.8 GPa assuming two Voigt functions for Yb^{2+}, and those for Yb^{3+} with arctan-like backgrounds. The intensities of the two arctan-like backgrounds were determined to be proportional to the intensities of their corresponding Voigt functions of the Yb^{2+} and Yb^{3+} components. The mean valence is defined to be v=2 + I(3+)/(I(2+) + I(3+)), where I(n+) is the intensity of Yb^{n+} component [43]. The Yb valences of YbCu, $YbCu_2$, and $YbCu_{6.5}$ at ambient pressure were estimated to be 2.05, 2.20, and 2.41, respectively. In $YbCu_2$ earlier magnetic and lattice constant measurements suggested the Yb valence of 2.4–2.5 [44, 45]. While the photoelectron spectroscopy (PES) showed nearly the divalent Yb state of 2.18 later [46]. Present bulk-sensitive measurement supports the PES result.

Pressure dependence of the Yb valence of YbCu and $YbCu_2$ is shown in Figs. 1 (e) and 1 (f), respectively. In YbCu we found the first-order valence transition around 4 GPa, and the change in the Yb valence is reduced above 5 GPa. Similarly, in $YbCu_2$ a rapid change in the Yb valence was observed at the pressure between 4 and 8 GPa, and further increase of the pressure does not change the Yb valence much above 8 GPa. Temperature-induced first-order valence transition of the Yb compounds has been observed in $YbInCu_4$ so far [43, 47, 48], but the first-order transition under pressure is rare.

In $YbCu_{6.5}$ we found an anomalous pressure-induced change in the Yb valence. The Yb valence decreased rapidly in the pressure range between 3–4 GPa from 2.42 to 2.1 and increased gradually with further increase of the pressure as shown in Fig. 1 (g). The magnetic Yb^{3+} state is favored commonly at high pressures in Yb compounds because of its smaller ionic radius of the Yb^{3+} ion compared with that of Yb^{2+} ion. The rare-earth metal theory predicted a return to the divalent state or to the valence fluctuation region under the pressure with increasing the pressure up to a few hundred GPa (Mbar range) [8], which has not been observed experimentally so far, despite trials up to 202 GPa in Yb metal [49]. Therefore, the decrease of the Yb valence at low pressures in $YbCu_{6.5}$ is highly anomalous, which cannot be understood by the conventional Anderson models. Recently, such pressure-induced anomalous valence crossover was found in $YbCu_{4.5}$, $YbCu_5$-based intermetallic compounds, and $YbInCu_4$-based compounds [9–11]. However, $YbCu_{4.5}$ showed a possible structural transition around the pressure of the valence transition, while $YbCu_{6.5}$ did not have a structural transition up to 17.4 GPa as shown below. The $YbCu_5$-based compounds also did not show any structural transition [10].

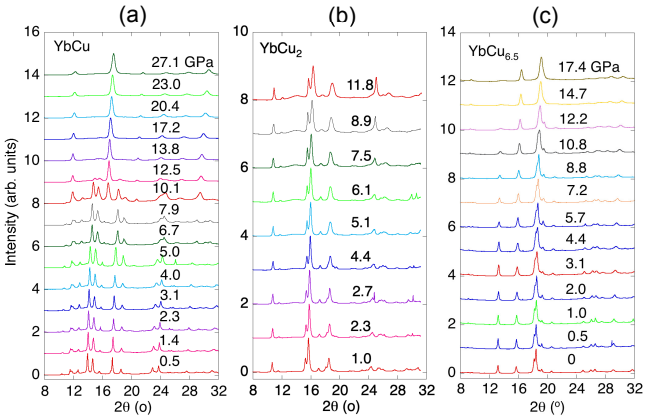

FIG. 2. (Color online) (a), (b), and (c) Pressure dependence of the XRD patterns for (a) YbCu, (b) $YbCu_2$, and (c) $YbCu_{6.5}$, respectively.

We also measured the temperature dependence of the PFY-XAS spectra of YbCu, $YbCu_2$, and $YbCu_{6.5}$ (the results are not shown here). No temperature dependence of the Yb valence was observed within errors in these compounds.

B. XRD under pressure

Figures 2 (a), 2 (b), and 2 (c) show the XRD patterns of of YbCu, $YbCu_2$, and $YbCu_{6.5}$as a function of pressure, respectively. In YbCu the first-order valence transition occurred at 4 GPa as described above, but there is no structural transition up to 7.9 GPa. On the other hand, the XRD pattern of YbCu in Fig. 2 (a) clearly demonstrates that a structural transition occurs at the pressure between 7.9 and 12.5 GPa. The high-pressure phase is most likely to be the cubic CsCl-type as will be described below. Interestingly, the pressure-dependent Yb-valence does not show a significant change in the pressure of the structural transition. In $YbCu_2$ the successive valence transition occurred around 4–7 GPa, while no structural phase transition was observed up to 11.8 GPa. In $YbCu_{6.5}$ no structural transition was also observed up to 17.4 GPa as shown in Fig. 2 (c). Thus, the first-order valence transition in YbCu, the successive valence transition in $YbCu_2$, and the anomalous decrease of the Yb valence at low pressure in $YbCu_{6.5}$ do not accompany the structural phase transition.

Figure 3 (a) shows a schematic view of the crystal structure of YbCu at lower pressures or at ambient pressure. Figures 3 (b)–3 (d) show the analyzed results of the XRD patterns in Fig. 2 (a). The change in the vol-

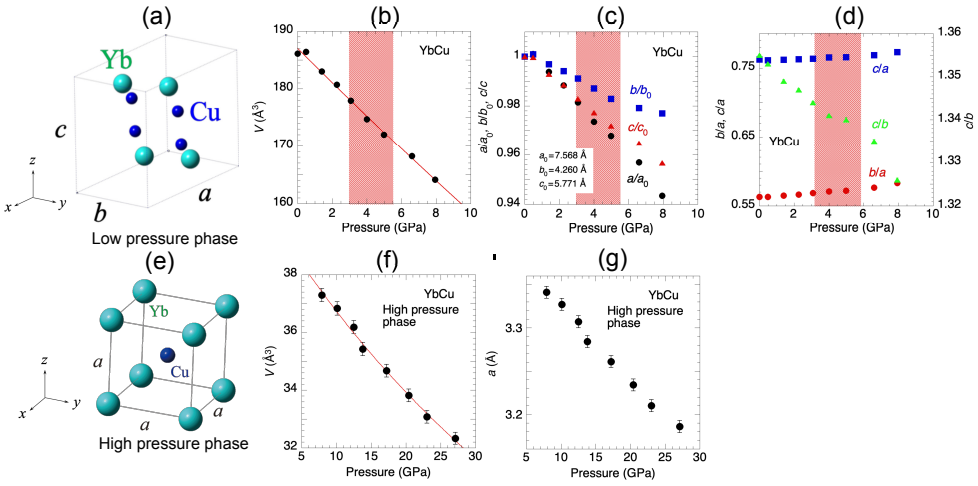

FIG. 3. (Color online) (a) A schematic view of the YbCu crystal structure at low pressures before the structural phase transition. (b) Pressure dependence of the volume at a low-pressure phase. A shaded area corresponds to the pressure range of the valence transition in Fig. 1 (e). (c) Pressure dependence of the normalized lattice parameters at a low-pressure phase. (d) Pressure dependence of the ratios of the lattice constants at a low-pressure phase. (e) A crystal structure at a high-pressure phase. (f) Pressure dependence of the volume at a high-pressure phase. (g) Pressure dependence of the lattice parameter at a high-pressure phase. For the data where the error is not visible, the error is less than or equal to the symbol size.

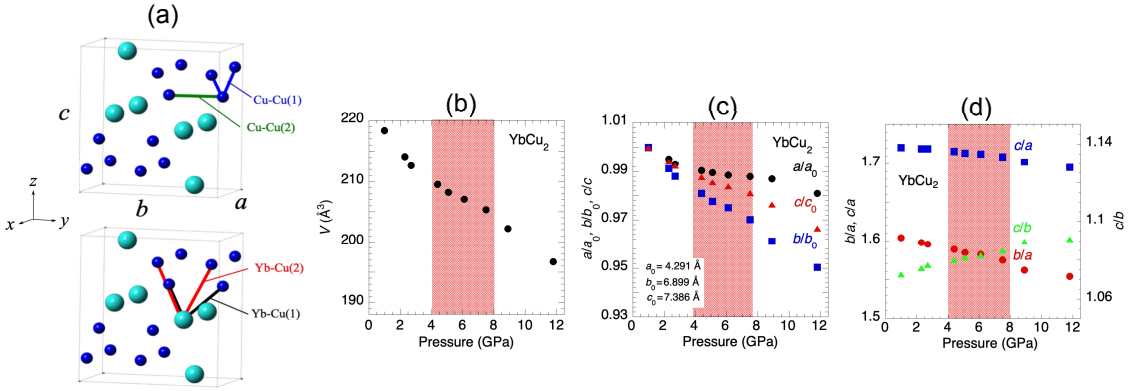

FIG. 4. (Color online) (a) A schematic view of the $YbCu_2$ crystal structure. (b) Pressure dependence of the volume. A shaded area around 4–8 G Pa corresponds to the pressure range of the valence transition in Fig. 1 (f). (c) Pressure dependence of the normalized lattice parameters. (d) Pressure dependence of the ratios of the lattice constants. For the data where the error is not visible, the error is less than or equal to the symbol size.

ume was linear to pressure, and there was no particular anomaly as shown in Fig. 3 (b). In Fig. 3 (c) it can be seen that compression along the b axis is less likely to occur than those along the a and c axes. This can be clearly seen in Fig. 3 (d), which shows the ratios of the lattice constants. The XRD patterns of the high-pressure phase after the structural phase transition in YbCu could be fitted with the CsCl-type crystal structure as shown in Fig. 3 (e). This is consistent with the crystal structures of RCu with R being the heavy rare-earth elements (Gd-Lu), for which the cubic CsCl-type (Pm-3m) is reported to be stable [25]. The only exception is YbCu, where the crystal structure is reported to be the orthorhombic FeB-type ($Pnma$) [18]. This is presumably attributed to the larger ionic size of Yb because of the nearly divalent state. Therefore, it is reasonable that the cubic CsCl-type YbCu is stabilized under high pressure. At high pressures above the structural phase transition, the volume and lattice constant decrease monotonically as shown in Figs. 3 (f) and 3 (g). In $YbInCu_4$ the first-order valence transition accompanied the structural phase transition [51]. On the other hand, in YbCu the structural phase transition starts to occur partially just above the pressure of the valence transition. This seems to suggest that the structural phase transition is triggered by the valence transition at the beginning of the structural transition, although the origin of the valence transition is not known.

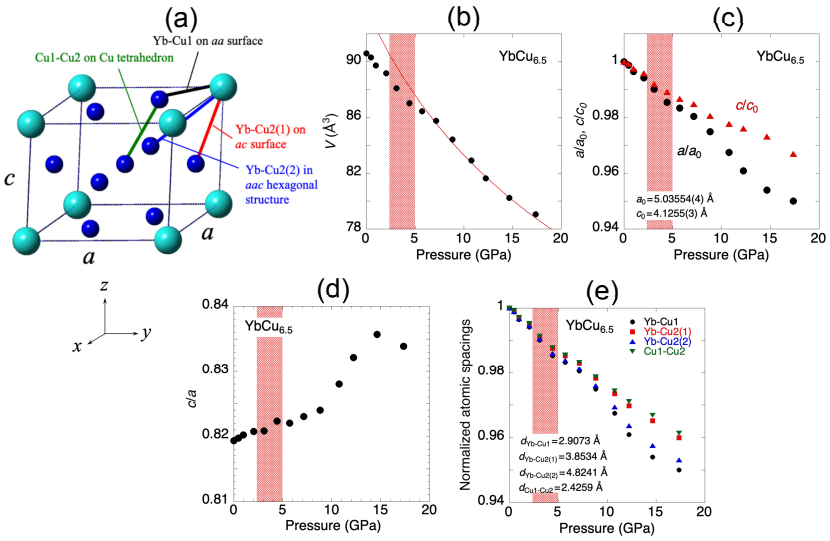

FIG. 5. (Color online) (a) A schematic view of the $YbCu_{6.5}$ crystal structure. Here, it is noted that the report of ref. [13] suggested that 18% of the Yb site was randomly occupied by Cu–Cu dimers (not shown in the figure). (b) Pressure dependence of the volume. A shaded area corresponds to the pressure range of the valence transition in Fig. 1 (f). (c) Pressure dependence of the normalized lattice parameters. (d) Pressure dependence of the ratio c/a of the lattice constants. (e) Pressure dependence of the normalized atomic spacing, where each distance is defined as shown in (a). For the data where the error is not visible, the error is less than or equal to the symbol size.

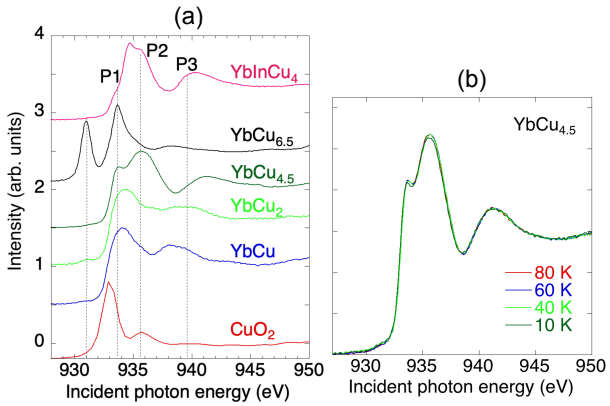

FIG. 6. (Color online) (a) XAS spectra of YbCu, $YbCu_2$, $YbCu_{4.5}$, $YbCu_{6.5}$, and $YbInCu_4$ at 10 K with that of Cu_2O at 300 K. (b) Temperature dependence of the XAS spectra of $YbCu_{4.5}$.

Figure 4 (a) shows a schematic view of the crystal structure of $YbCu_2$. Figures 4 (b)–4 (d) show the analyzed results of the XRD patterns in Fig. 2 (b). The volume drops gradually in the pressure range where the successive change in the Yb-valence occurs as shown in Fig. 4 (b). The lattice constant in Fig. 4 (c) also changes in the same way as the volume changes. $YbCu_2$ is compressed strongly along the b axis than along the a and c axes. This change can be clearly seen in the ratio between the axes in Fig. 4 (d). The changes in the positions of Yb_z, Cu_y, and Cu_z are shown in Figs. S3 (b), and S3 (c) in the Supplementary material [25]. Since the XRD peaks were broader in the high-pressure range and reliable results could not be obtained, the analyzed results of the atomic position and the atomic distance are shown only up to 9 GPa. The atomic position of Yb_z rises above about 7 GPa. The tendency of the change in the position of Cu in Fig. S3 (c) is not clear. Each atomic distance decreases with pressure as shown in Fig. S3 (d), where pressure-induced changes are smaller or more stable at 6–9 GPa than the case less than 6 GPa [25]. In the pressure region where the valence transition occurs, the change in the position of Cu becomes small, and Yb shifts along the z direction. No structural phase transitions have been observed in $YbCu_2$ in the pressure range measured, but these anomalous changes in volume and atomic position correlate to the valence transition.

Figure 5 (a) shows a schematic view of the crystal structure of $YbCu_{6.5}$. Figures 5 (b)–5 (e) show the analyzed results of the XRD patterns in Fig. 2 (c). Figures 5 (b)–5 (e) indicate that in $YbCu_{6.5}$ volume, normalized lattice constants, a ratio of the lattice constants, and the atomic spacings, respectively. We analyzed the XRD patterns of $YbCu_{6.5}$ with the Rietveld method and fitted in the all pressure range with the same crystal structure. The XRD patterns of $YbCu_{6.5}$ slightly changed above 12.2 GPa. This may be due to the non-hydrostatic condition by solidification of the pressure-transmitting medium which resulted in the peaks being broader. The crystal structure seems not to show a significant change around 3–4 GPa where the anomalous valence transition was observed. The c/a ratio of the lattice constants in

Fig. 5 (d) is a gradual change up to around 10 GPa, but it rises sharply at higher pressures above 10 GPa. This corresponds to a larger compressibility along the a axis compared to that along the c axis. Atomic distances also show similar changes to the volume and lattice constants as shown in Fig. 5 (e).

The crystal of $YbCu_{6.5}$ is characteristic with respect to the Yb-Cu distances. There are two kinds of Cu sites, Cu1 and Cu2, and the distance of Yb-Cu1 is much smaller than those of Yb-Cu2(1) and Yb-Cu2(2). Therefore, the hybridization between Yb and Cu may have a strong Cu site dependence in $YbCu_{6.5}$. The trend of the distances between Yb-Cu2(2) and Yb-Cu1 to decrease with pressure is different from those between Yb-Cu2(1) and Cu1-Cu2 as shown in Fig. 5 (e). The former distances, Yb-Cu1 and Yb-Cu2(2) are on the aa surface and in the aac-hexagonal structure, respectively, as shown in Fig. 5 (a). The latter distances, Yb-Cu2(1) and Cu1-Cu2 are on the ac surface and on the Cu tetrahedron, respectively. The distances of Yb-Cu1 and Yb-Cu2(2) start to decrease more rapidly above around 10 GPa. Pressure dependences of the lattice constants of a in Fig. 5 (c) also show a more rapid decrease above 10 GPa compared to that of c. These pressure-induced changes in the distances of Yb-Cu1 and Yb-Cu2(2) reflect that in the lattice constant a. These changes seem to be correlated to those in the Yb valence above 10 GPa. Thus, the pressure-induced change in the Yb-Cu distances could be the origin of the increase of the Yb valence above 10 GPa in $YbCu_{6.5}$.

No structural phase transition was observed in $YbCu_{6.5}$ up to 17.4 GPa, including the pressure range around 3–4 GPa. The valence gradually increases with pressure above 10 GPa, and this normal change corresponds to the rapid increase of the ratio of the lattice in Fig. 5 (d). On the other hand, pressure-induced change in the valence up to 10 GPa without structural phase transition is anomalous. We could consider a following scenario. Pressure-induced changes in the volume and lattice constant along the a axis become sharp above 7 GPa as shown in Figs. 5 (b) and 5 (c). Since the ionic radius of Yb^{3+} is smaller than that of Yb^{2+}, the transition to the Yb^{3+} state above 7 GPa is normal. In contrast, the change in the ratio of the lattice constants is gradual up to 10 GPa as shown in Fig. 5 (d). The pressure dependence of the volume seems to be also gradual in the pressure range of 4–7 GPa, which may correspond to decompression as discussed in Ref. [11], when we consider the volume change above 7 GPa is a normal compression, consequently, this possibly cause a decrease in the valence in this pressure range. However, the more direct reason for this anomalous valence transition is likely to be derived from the electronic structure of Cu above the Fermi level, the coexistence of two kinds of charge states of Cu, which are described below. In $YbCu_{6.5}$, it is also likely to occur that the atomic distance between the Cu–Cu dimer site which replaces the 18% of the Yb site has changed by pressure [13], leading to the charge transfer from the Cu–Cu dimer to the Yb site. Unfortunately, the present resolution of the XRD patterns under pressure did not allow us to refine the atomic position of the Cu–Cu dimer site.

In Figs. 3 (b), 3 (f), and 5 (b) we show fits of the pressure-volume relation by using an empirical formula of the Murnaghan's equation of state [52], $\frac{V}{V_0} = [1 + p\frac{B'}{B_0}]^{-\frac{1}{B'}}$, where p, V, V_0, B_0, and B' are pressure, volume, volume at ambient pressure, bulk modulus of incompressibility, and fits first derivative with respect to the pressure, respectively. In Fig. 5 (b) we fitted for the data above 8.8 GPa far above the valence transition pressure. We obtain the parameters of $B_0 = 61.98$ GPa, $B' = -0.301$, $V_0 = 187.0$ Å^3 for YbCu at the low-pressure phase, $B_0 = 61.98$ GPa, $B' = 1,65$, $V_0 = 40.3$ Å^3 for YbCu at the high-pressure phase, and $B_0 = 59.96$ GPa, $B' = 5.34$, $V_0 = 101.2$ Å^3 for $YbCu_{6.5}$. A small negative value of B' in YbCu is due to the nearly linear pressure dependence of the volume.

The temperature-induced first-order valence transition of $YbInCu_4$ had been believed not to accompany the structural transition [48, 53]. However, later, it was found that the splitting of Bragg peaks at the 2θ angle greater than 90° was detected in high-order reflections below the Yb valence transition temperature in a single-crystal XRD experiment, indicating a structural change from a $F\bar{4}3m$-cubic to a $I\bar{4}m2$-tetragonal structure [51]. The present measurements for the $YbCu_x$ systems were performed for the powder samples and thus precise measurements of the XRD patterns for the single crystals under pressure have a potential to show a change in the crystal structure. This remains a challenge to study in the future.

C. XAS at Cu L absorption edge

Complementary to the measurements of the electronic structure of the Yb site, we measured the high-resolution XAS spectra of the Cu site at the Cu-L_3 absorption edge for YbCu, $YbCu_2$, $YbCu_{4.5}$, $YbCu_{6.5}$, and $YbInCu_4$ at 10 K with that for Cu_2O at 300 K as shown in Fig. 6 (a). Both spectra of YbCu and $YbCu_2$ are similar to each other. The spectrum of Cu_2O reproduced well the previous results [54]. The single peak around 933 eV in Cu_2O was assigned to a $2p^53d^{10}$ final state coming from a $2p^63d^9$ initial state [55]. The spectra of $YbCu_x$ are very different from that of Cu_2O, where Cu atoms are covalently bonded to the O atoms [54, 56, 57], but are similar to that of Cu metal [54] except $YbCu_{6.5}$. Theoretical calculations for fcc and bcc Cu metal suggested that the peak P2 at 935 eV and the peak P3 at 939 eV correspond to the transitions of $2p$–$3d$ and $2p$–$4s$, respectively [56]. The energy of the absorption edge shifts to higher energy at the order of YbCu < $YbCu_2$ < $YbCu_{4.5}$.

In $YbInCu_4$ a slight shift of the peak P2 to higher energy was observed with increasing the intensity of the peak P1 below the temperature of the valence transition,

where the weak shoulder peak P1 was considered to be derived from the Cu 3d states [58]. It was suggested that the electron transfer from the Cu 3d sites to the Yb 4f sites occurred across the valence transition at low temperatures, resulting in the increase of the DOS of the Yb^{2+} states near the Fermi level. The peak intensity of YbCu and $YbCu_2$ corresponding to the peak P1 of $YbInCu_4$ is relatively stronger than that of $YbCu_{4.5}$. This suggests that the unoccupied states of Cu 3d of the former compounds are larger than those of the latter. This explains why the Yb valences of YbCu and $YbCu_2$ are smaller than that of $YbCu_{4.5}$.

The electronic structure of Cu in $YbCu_{6.5}$ above the Fermi level is very different from others as shown in Fig. 6 (a), and rather similar to that of K_2NaCuF_6 [59]. $YbCu_{6.5}$ has a sharp and strong peak at 931 eV, which was not observed in YbCu, $YbCu_2$, and $YbCu_{4.5}$. Two peaks around 931 eV and 934 eV could be assigned to be Cu^{2+} and Cu^{3+} states [57, 60]. In $YbCu_{6.5}$ the XAS spectrum in Fig. 6 (a) is likely to be a sum of the three different electronic states of Cu because of the three kinds of the Cu sites (2c, 3g, and dimer Cu atoms at vacant Yb sites) [13]. The peak at 931 eV observed only for $YbCu_{6.5}$ is possibly caused by the Cu dimer site or one of the Cu sites in Fig. 5 (a). A weak shoulder peak on the right of the 934 eV peak in $YbCu_{6.5}$ is due to the multiplet effect.

The Yb valence drastically decreased with pressure at low pressures in both $YbCu_{4.5}$ and $YbCu_{6.5}$ compounds [9]. In $YbCu_{4.5}$ the rapid decrease of the valence was considered to be caused by the structural phase transition [9]. However, there is no structural phase transition in $YbCu_{6.5}$ and the electronic structure of the Cu site of $YbCu_{6.5}$ is different from that of $YbCu_{4.5}$. X-ray absorption occurs for the unoccupied states above the Fermi level and the Fermi level corresponds to approximately the absorption edge of the XAS spectrum in the metallic compounds. Thus, the results may suggest a lower Fermi level in $YbCu_{6.5}$ compared to other $YbCu_x$ compounds and it may correspond to the valence transition at a very low pressure of 3–4 GPa. We could consider a possible scenario for the valence transition in $YbCu_{6.5}$. When pressure is applied, the 4f level of the Yb^{2+} component shifts to the upper 5d band, and the charge transfer from the Yb 4f band to the 5d band occurs, resulting in the increase in the Yb valence normally [25, 61, 62]. However, the present results suggest that the inverse charge transfer from the Cu^{2+} to the Yb^{3+} bands with pressure possibly occurs. A similar charge transfer from Cu to Yb was reported in $YbInCu_4$, where the first-order valence transition was induced by decreasing the temperature and the Yb valence deceased toward the divalent state [58]. It is noted that figure 5 shows the lattice constants and the Yb-Cu and Cu-Cu distances decrease with pressure without a modification and the c/a ratio does not show a significant pressure dependence around the pressure range of the valence transition. Therefore, this valence transition may not be caused by the anomaly in the crystal structure. In $YbCu_{6.5}$ the existence of the Cu^{2+} state, the three kinds of Cu sites, and the electronic structure may play an important role in the anomalous valence transition. A theoretical study is desired to understand the exact mechanism of the anomalous valence transition in $YbCu_{6.5}$. Figure 6 (b) shows the temperature dependence of the XAS spectra of $YbCu_{4.5}$ below 80 K. No temperature dependence was observed. In $YbCu_{4.5}$ the Yb valence decreased with decreasing the temperature from 2.94 at 100 K to 2.92 at 16 K [9]. The result in Figure 6 (b) indicates that the temperature-induced change in the electronic structure of the Cu sites is too small to observe in the present resolution.

IV. CONCLUSION

The electronic and crystal structures of YbCu, $YbCu_2$, and $YbCu_{6.5}$ under pressure were measured by the high-resolution x-ray absorption spectroscopy and x-ray diffraction. A first-order valence transition was found at 4 GPa in YbCu where no structural phase transition was observed. In YbCu the structural transition from the FeB-type to CsCl-type crystal structure around 10 GPa was found, whereas the Yb valence does not show a significant increase between 10–15 GPa, and it seems to show a small step-like increase of the valence at 15 GPa. Anomalies in pressure-induced valence changes in these systems have been found to correspond to anomalies in the lattice constants and atomic distances in YbCu and $YbCu_2$. In $YbCu_{6.5}$ pressure-induced anomalous valence transition was observed at low pressure, also without the structural transition. The Yb valence decreased approximately from 2.41 at 2.2 GPa to 2.1 at 5.1 GPa and increased gradually with further increase of the pressure. No anomaly in the crystal structure was observed in this pressure range.

The electronic structures of the Cu site of $YbCu_x$ were also measured at the Cu-L_3 absorption edge at ambient pressure by x-ray absorption spectroscopy. The XAS spectra of YbCu and $YbCu_2$ are similar, but that of $YbCu_{6.5}$ was very different from others. In $YbCu_{6.5}$ a possibility of a charge transfer from Cu d to Yb 4f bands was discussed as an origin of the anomalous decrease in the Yb valence in $YbCu_{6.5}$ at low pressures. It was shown that the Cu-site-dependent decrease of the atomic distances could be an origin of the increase of the Yb valence above 10 GPa. We also measured the valence band spectra of $YbCu_x$, supporting the results of the PFY-XAS spectra for the Yb valence.

In $YbCu_x$, the crystal structure changed when the Cu composition was changed. We observed large pressure-induced valence changes despite the absence of a crystalline phase transition. But it is common that anomalous changes in the Yb valences were linked to anomalies in crystal structures.

ACKNOWLEDGMENTS

The experiments were performed at Taiwan beamlines BL12XU and BL12B2 at SPring-8 under Proposals Nos. 2017B4260, 2017B4267, 2018A4258, and 2018A4141 (corresponding proposal Nos. 2017-2-179, 2018-1-039, 2018-1-012, and 2018-2-267 of NSRRC) and also beamlines BL-7 and BL-14 at HiSOR under Proposals Nos. 17AG009 and 18AG003. We thank the N-BARD, Hiroshima University for supplying the liquid helium. This work is supported by Grants in Aid for Scientific Research from the Japan Society for the Promotion of Science (Kiban Houga 18K18743).

[1] K. H. J. Buschow, Intermetallic compounds of rare earths and non-magnetic metals, Rep. Prog. Phys. **42**, 1373 (1979).

[2] J. M. Lawrence, P. S. Riseborough, and R. D. Parks, Valence fluctuation phenomena, Rep. Prog. Phys. **44**, 1 (1981).

[3] P. Strang, A. Svane, W. M. Temmerman, Z. Szotek, and H. Winter, Understanding the valency of rare earths from first-principles theory, Nature **399**, 756 (1999).

[4] K. Kummer, C. Geibel, C. Krellner, G. Zwicknagl, C. Laubschat, N. B. Brookes, and D V. Vyalikh, Similar temperature scale for valence changes in Kondo lattices with different Kondo temperatures, Nat. Commun. **9**, 2011 (2018).

[5] H. v. Löhneysen, A. Rosch, M. Vojta, and P. Wölfle, Fermi-liquid instabilities at magnetic quantum phase transitions, Rev. Mod. Phys. **79**, 1015 (2007).

[6] N. E. Bickers, D. L. Cox, and J. W. Wilkins, Self-consistent large-N expansion for normal-state properties of dilute magnetic alloys, Phys. Rev. B **36**, 2036 (1987).

[7] S. Doniach, The Kondo lattice and weak antiferromagnetism, Physica B & C **91**, 231 (1977).

[8] J. F. Herbst and J. W. Wilkins, Pressure-induced $4f$ occupancy enhancement in the rare-earth metals, Phys. Rev. B **29**, 5992, (1984).

[9] H. Yamaoka, N. Tsujii, Y. Yamamoto, Y. Michiue, J.-F. Lin, N. Hiraoka, H. Ishii, K.-D. Tsuei, and J. Mizuki, Reentrant valence transition in $YbCu_{4.5}$ under pressure, Phys. Rev. B **97**, 085106 (2018).

[10] H. Yamaoka, N. Tsujii, M.-T. Suzuki, Y. Yamamoto, I. Jarrige, H. Sato, J.-F. Lin, T. Mito, J. Mizuki, H. Sakurai, O. Sakai, N. Hiraoka, H. Ishii, K.-D. Tsuei, M. Giovannini, and E. Bauer, Pressure-induced anomalous valence crossover in cubic $YbCu_5$-based compounds, Scie. Rep. **7**, 5846 (2017).

[11] H. Yamaoka, A. Ohmura, N. Tsujii, Y. Furue, H. Ishii, and N. Hiraoka, Electronic and crystal structures of $YbInCu_4$-based compounds under pressure, J. Phys. Soc. Jpn. **92**, 064704 (2023).

[12] A. Iandelli and A. Palenzona, The ytterbium-copper system, J. Less-Common Metals **25**, 333 (1971).

[13] J. Hornstra and K. H. J. Buschow, The crystal strucure of $YbCu_{6.5}$, J. Less-Common Metals **27**, 123 (1972).

[14] M. Giovannini, R. Pasero, S. De Negri, and A. Saccone, Yb(Cu, T)$_5$ and Yb(Cu, T)$_{4.5}$ solid solutions (T = Ag, Au, Pd), Intermetallics **16**, 399 (2008).

[15] L. Spendeler, D. Jaceard, J. Sierro, M. François, A. Stepanov, and J. Voiron, Resistivity and thermoelectric power of $YbCu_{4.5}$ under very high pressure, J. Low Temp. Phys. **94**, 585 (1994).

[16] N. Tsujii, J. He, F. Amita, K. Yoshimura, K. Kosuge, H. Michor, G. Hilscher, and T. Goto, Kondo-lattice formation in cubic-phase $YbCu_5$, Phys. Rev. B **56**, 8103, (1997).

[17] D. Debray, B. F. Wortmann, and S. Methfessel, Anomalous magnetic susceptibility behavior of some Yb compounds: Thermally excited interconfiguration crossover, Phys. Rev. B **9**, 4009, (1976).

[18] B. D. Belan, O. I. Bodak, R. Ceny, J. V. Pacheco, and K. Yvon, Crystal structure of ytterbium copper, YbCu, Zeitschrift f'ur Kristallographie - New Crystal Structures **212**, 508 (1997).

[19] D. Jaccard, A. Junod, and J. Sierro, Electrical resistivity, thermopower and specific heat of the intermediate valence system $YbCu_x$, Helv. Phys. Acta **53**, 583 (1980).

[20] R. Černý, M. François, K. Yvon, D. Jaccard, E. Walker, V. Petříček, I. Císařová, H.-U. Nissenk, and R. Wessicken, A single-crystal x-ray and HRTEM study of the heavy-fermion compound $YbCu_{4.5}$, J. Phys.: Condens. Matter **8**, 4485 (1996).

[21] A. Amato, R. A. Fisher, N. E. Phillips, D. Jaccard, and E. Walker, Magnetic field dependence of the specific heat of heavy-fermion $YbCu_{4.5}$, Physica B **165-166**, 389 (1990).

[22] K. Hämäläinen, D. P. Siddons, J. B. Hastings, and L. E. Berman, Elimination of the inner-shell lifetime broadening in x-ray-absorption spectroscopy, Phys. Rev. Lett. **67**, 2850 (1991).

[23] K. Hämäläinen, C. C. Kao, J. B. Hasting, D. P. Siddons, L. E. Berman, V. Stojanoff, and S. P. Cramer, Spin-dependent x-ray absorption of MnO and MnF_2, Phys. Rev. B **46**,14274 (1992).

[24] H. Yamaoka, Pressure dependence of the electronic structure of $4f$ and $3d$ electron systems studied by x-ray emission spectroscopy, High Press. Res. **36**, 262 (2016).

[25] See Supplemental Materials [url] will be given by the editor side], which includes Refs. [9, 18, 20, 27, 46, 62–68]. A f electron number dependence of the volume for the LnCu (Ln: lanthanoid) family and the fit examples to the XRD patterns are shown. Details of a promotional model are also described.

[26] D. Jaccard, F. Haenssler, and J. Sierro, Pressure dependence of electrical resistivity and thermopower: Valence transition in $YbCu_2$ and TmSe, Helv. Phys. Acta **53**, 590 (1980).

[27] H. Yamaoka, I. Jarrige, N. Tsujii, N. Hiraoka, H. Ishii, and K-D. Tsuei, Temperature dependence of the Yb valence in $YbCu_5$ and $YbCu_{5-x}Al_x$ Kondo compounds studied by x-ray spectroscopy, Phys. Rev. B **80**, 035120 (2009).

[28] N. Sato, H. Abe, M. Kontani, S. Yamagata, K. Adachi, and T. Komatsubara, Magnetic properties of heavy fermion compounds $YbCu_{3.5}$ and $YbCu_{4.5}$, Physica B **163**, 325 (1990).

[29] J. C. P. Klasse, F. R. de Boer, and P. F. de Chatel, Systematics in intermetallic compounds containing intermediate-valent ytterbium, Physica B+C **106**, 178 (1981).

[30] Z. Fisk, J. D. Thompson, and H. R. Ott, Heavy-electrons: New materials, J. Magn. Magn. Mater. **76-77**, 637 (1988).

[31] C. Rossel, K. N. Yang, M. B. Maple, Z. Fisk, E. Zirngiebl, and J. D. Thompson, Strong electronic correlations in a new class of Yb-based compounds: $YXCu_4$ (X = Ag, Au,Pd), Phys. Rev. B **35**, 1914 (1987).

[32] A. Amato, R. A. Fisher, N. E. Phillips, D. Jaccard, and E. Walker, Pressure dependence of the specific heat of heavy-fermion $YbCu_{4.5}$, Physica B **165-166**, 425-426 (1990).

[33] S. Gottlieb-Schönmeyer, S. Brühne, F. Ritter, W. Assmus, S. Balanetskyy, M. Feuerbacher, T. Weber, and W. Steurer, Crystal growth of copper-rich ytterbium compounds: The predicted giant unit cell structures $YbCu_{4.4}$ and $YbCu_{4.25}$, Intermetallics **17**, 6 (2009).

[34] P. Popčević, I. Smiljanić, N. Barišić, A. Smontara, J. Dolinšek, and S. Gottlieb-Schönmeyer Transport properties of $YbCu_{4.4}$ giant-unit-cell metallic compound, Croat. Chem. Acta **83**, 69 (2010).

[35] H. Yamaoka, I. Jarrige, N. Tsujii, J.-F. Lin, N. Hiraoka, H. Ishii, and K.-D. Tsuei, Temperature and pressure-induced valence transitions in $YbNi_2Ge_2$ and $YbPd_2Si_2$, Phys. Rev. B **82**, 035111 (2010).

[36] H. K. Mao and P. M. Bell, High-pressure physics: The 1-megabar mark on the Ruby R_1 static pressure scale, Science **191**, 852 (1976).

[37] K. Syassen, Ruby under Pressure, High Pressure Res. **28**, 75 (2008).

[38] A. P. Hammersley, S. O. Svensson, M. Hanfland, A. N. Fitch, and D. Hausermann, Two-dimensional detector software: From real detector to idealised image or two-theta scan, High Press. Res. **14**, 235 (1996).

[39] H. M. Rietveld, A profile refinement method for nuclear and magnetic structures, J. Appl. Cryst. **2**, 65 (1969).

[40] A. Le Bail, H. Duroy and J. L. Fourquet, Ab-initio structure determination of $LiSbWO_6$ by X-ray powder diffraction, Mater. Res. Bull. **23**, 447 (1998).

[41] Jana2006 program to analyze the crystal structures.

[42] M. Sawada, K. Yaji, M. Nagira, A. Kimura, H. Namatame, and M. Taniguchi, Design concept and performance of the soft x-ray beamline HiSOR-BL14, AIP Conf. Proc. **879**, 551 (2007).

[43] H. Yamaoka, N. Tsujii, K. Yamamoto, A. M. Vlaicu, H. Oohashi, H. Yoshikawa, T. Tochio, Y. Ito, A. Chainani, and S. Shin, Systematic study of bulk sensitive spectroscopy in the valence transition of $YbInCu_4$-based compounds, Phys. Rev. B **78**, 045127 (2008).

[44] J. C. P. Klaasse, W. C. M. Mattens, F. R. de Boer, and P. F. de Cllatel, Ambiguous magnetic behaviour of some Yb-compounds, Physica B+C **86-88**, 234 (1977)

[45] D. Debray, Crystal chemistry of the $CeCu_2$-type structure, J. Less-Common Met. **30**,237 (1973).

[46] A. Fujimori, T. Shimizu, and H. Yasuoka, Photoemission study of valence fluctuation in $YbCu_2$, Phys. Rev. B **35**, 8945 (1987).

[47] I. Felner and I. Nowik, First-order valence phase transition in cubic $Yb_xIn_{1-x}Cu_2$, Phys. Rev. B **33**, 617 (1986).

[48] H. Sato, K. Shimada, M. Arita, K. Hiraoka, K. Kojima, Y. Takeda, K. Yoshikawa, M. Sawada, M. Nakatake, H. Namatame, M. Taniguchi, Y. Takata, E. Ikenaga, S. Shin, K. Kobayashi, K. Tamasaku, Y. Nishino, D. Miwa, M. Yabashi, and T. Ishikawa, Valence transition of $YbInCu_4$ observed in hard x-ray photoemission spectra, Phys. Rev. Lett. **93**, 246404 (2004).

[49] G. N. Chesnut and Y. K. Vohra, Structural and electronic transitions in Ytterbium metal to 202 GPa. Phy. Rev. Lett. **82**, 1712, (1999).

[50] J. M. Lawrence, P. S. Riseborough, C. H. Booth, J. L. Sarrao, J. D. Thompson, and R. Osborn, Slow crossover in $YbXCu_4$ (X = Ag, Cd, In, Mg, Tl, Zn) intermediate-valence compounds, Phys. Rev. B **63**, 054427 (2001).

[51] S. Tsutsui, K. Sugimoto, R. Tsunoda, Y. Hirose, T. Mito, R. Settai, and M. Mizumaki, First-order structural change accompanied by Yb valence transition in $YbInCu_4$, J. Phys. Soc. Jpn. **85**, 063602 (2016).

[52] F. D. Murnaghan, The compressibility of media under extreme pressures, Proc. Natl. Acad. Sci. U.S.A. **30**, 244 (1944).

[53] Y. Utsumi, H. Sato, C. Moriyoshi, Y. Kuroiwa, H. Namatame, M. Taniguchi, K. Hiraoka, K. Kojima, and K. Sugimoto, Synchrotron radiation diffraction study of $YbInCu_4$, Jpn. J. Appl. Phys. **50**, 05FC10 (2011).

[54] M. Finazzi, G. Ghiringhelli, O. Tjernberg, Ph. Ohresser, and N. B. Brookes, Radiationless Raman versus Auger behavior at the Cu L_3 resonance of CuO and Cu_2O, Phys. Rev. B **61**, 4629 (2000).

[55] M.-J. Huang, G. Deng, Y. Y. Chin, Z. Hu, J.-G. Cheng, F. C. Chou, K. Conder, J.-S. Zhou, T.-W. Pi, J. B. Goodenough, H.-J. Lin, and C. T. Chen, Determination of hole distribution in $Sr_{14-x}Ca_xCu_{24}O_{41}$ using soft x-ray absorption spectroscopy at the Cu L_3 edge, Phys. Rev. B **88**, 014520 (2013).

[56] H. Ebert, J. Stöhr, S. S. P. Parkin, M. Samant, and A. Nilsson, L-edge x-ray absorption in fcc and bcc Cu metal: Comparison of experimental and first-principles theoretical results, Phys. Rev. B **53**, 16067 (1996).

[57] P. Jiang, D. Prendergast, F. Borondics, S. Porsgaard, L. Giovanetti, E. Pach, J. Newberg, H. Bluhm, F. Besenbacher, and M. Salmeron, Experimental and theoretical investigation of the electronic structure of Cu_2O and CuO thin films on Cu(110) using x-ray photoelectron and absorption spectroscopy, J. Chem. Phys. **138**, 024704 (2013).

[58] Y. Utsumi, H. Sato, H. Kurihara, H. Maso, K. Hiraoka, K. Kojima, K. Tobimatsu, T. Ohkochi, S.-I. Fujimori, Y. Takeda, Y. Saitoh, K. Mimura, S. Ueda, Y. Yamashita, H. Yoshikawa, K. Kobayashi, T. Oguchi, K. Shimada, H. Namatame, and M. Taniguchi, Conduction-band electronic states of $YbInCu_4$ studied by photoemission and soft x-ray absorption spectroscopies, Phys. Rev. B **84**, 115143 (2011).

[59] C. De Nadaï. Demourgues, and J. Grannec, $L_{2,3}$ x-ray absorption spectroscopy and multiplet calculations for KMF_3 and K_2NaMF_6 (M = Ni,Cu), Phys. Rev. B **63**, 125123 (2001).

[60] J. Ghijsen, L. H. Tjeng, J. van Elp, H. Eskes, J. Westerink, G. A. Sawatzky, and M. T. Czyzyk, Electronic structure of Cu_2O and CuO, Phys. Rev. B **38**, 11322 (1988).

[61] E. R. Ylvisaker, J. Kuneš, A. K. McMahan, and W. E. Pickett, Charge fluctuations and the valence transition in Yb under pressure, Phys. Rev. Lett. **102**, 246401

(2009).
[62] I. Jarrige, H. Yamaoka, J.-P. Rueff, J.-F. Lin, M. Taguchi, N. Hiraoka, H. Ishii, K.-D. Tsuei, K. Imura, T. Matsumura, A. Ochiai, H. S. Suzuki, and A. Kotani, Unified understanding of the valence transition in the rare-earth monochalcogenides under pressure, Phys. Rev. B **87**, 115107 (2013).
[63] H. Yamaoka, P. Thunström, N. Tsujii, I. Jarrige, K. Shimada, M. Arita, H. Iwasawa, H. Hayashi, J. Jiang, H. Namatame, M. Taniguchi, N. Hiraoka, H. Ishii, K.-D. Tsuei, M. Giovannini, and E. Bauer, The electronic structure and the valence state of Yb_2Pd_2Sn and $YbPd_2Sn$ studied by photoelectron and resonant x-ray emission spectroscopies, Phys. Rev. B **86**, 085137 (2012).
[64] G. A. Costa, E. A. Franceschi, and A. Tawansi, Phase equilibria in the EuCu system, J. Less Common Metals **106**, 175 (1985).
[65] C. C. Chao, H. L. Luo, and P. Duwez, CsCl-Type Compounds in Binary Alloys of Rare-Earth Metals with Zinc and Copper, J. Appl. Phys. **35**, 257 (1964).
[66] V. F. Degtyareva, F. Porsch, S. S. Khasanov, V. Sh. Shekhtman, and W. B. Holzapfel, Effect of pressure on structural properties of intermetallic LnM lanthanide compounds, J. Alloys & Compds. **246**, 248 (1997).
[67] R. Caputo, C. Oran, A. Tekin, and P. Villars, Equiatomic binary phases of Copper-Rare Earth Elements. An overview of monocuprides from first-principles calculations, ChemPhysChem. **24**, e202200718 (2023).
[68] H. Mizoguchi, J. Bang, T. Inoshita, T. Kamiya, and H. Hosono, On the origin of the negative thermal expansion behavior of YCu, Inorg. Chem. **58**, 11819 (2019).